Constraining Fault Friction and Stability with Fluid-Injection Field Experiments

Stacy Larochelle[1], Nadia Lapusta[1,2], Jean-Paul Ampuero[3], and Frédéric Cappa[3,4]

[1] Division of Geological and Planetary Sciences, California Institute of Technology, Pasadena, California 91125, USA.

[2] Division of Engineering and Applied Science, California Institute of Technology, Pasadena, California 91125, USA

[3] Université Côte d'Azur, IRD, CNRS, Observatoire de la Côte d'Azur, Géoazur, 06560 Sophia Antipolis, France

[4] Institut Universitaire de France, Paris, France

Corresponding author: Stacy Larochelle (stacy.larochelle@caltech.edu)

Key Points:

- Multiple frictional models with different stability reproduce the slip observed during the pressurization stage of a field experiment

- The depressurization phase provides additional constraints on hydromechanical parameters and hence fault stability

- Fault stability and the spatial extent of slip relative to the pressurized region depend on residual friction vs initial stress levels

Abstract

While the notion that injecting fluids into the subsurface can reactivate faults by reducing frictional resistance is well established, the ensuing evolution of slip is still poorly understood. What controls whether the induced slip remains stable and confined to the fluid-affected zone or accelerates into a runaway earthquake? Are there observable indicators of the propensity to earthquakes before they happen? Here, we investigate these questions by modeling a unique fluid-injection experiment on a natural fault with laboratory-derived friction laws. We show that a range of fault models with diverging stability with sustained injection reproduce the slip measured during pressurization. Upon depressurization, however, the most unstable scenario departs from the observations, suggesting that the fault is relatively stable. The models could be further distinguished with optimized depressurization tests or spatially distributed monitoring. Our findings indicate that avoiding injection near low-residual-friction faults and depressurizing upon slip acceleration could help prevent large-scale earthquakes.

Plain Language Summary

Fluid injections into the Earth's crust are common practice in the exploitation of subsurface energy ressources such as geothermal energy, shale gas and conventional hydrocarbons. These injections can perturb nearby fault structures and hence induce earthquakes and transient slow slip. Understanding what controls the stability (i.e., the propensity to generate earthquakes) and spatial extent of the fault response as well as identifying precarious faults is crucial to minimize the seismic hazard associated with these industrial practices. Here, we take a step towards this goal by modeling a unique experiment in which water was injected into a natural fault and the resulting slip measured directly at depth. We first show that multiple models can explain the observations equally well while pressure is increased in the experiment. In these

models, how stable the fault response is with further injection and how large of a zone is reactivated compared to the fluid-affected region depends on frictional properties. We then demonstrate that the slow slip response to a decrease in injection pressure further constrains the range of admissible models. Our work suggests that it may be possible to identify potentially hazardous faults with optimally designed injection tests without inducing damaging earthquakes.

1 Introduction

Earthquakes induced by fluid injection into the subsurface pose a major challenge for the geoenergy industry and society in general (Ellsworth, 2013; Grigoli et al., 2017). Tectonically-quiescent regions where dormant faults could be reactivated are particularly challenging, as their infrastructure was not designed for large-magnitude induced earthquakes (McGarr et al., 2015). At the same time, some faults have been observed to slip stably at aseismic speeds of $10^{-7} - 10^{-2}$ m/s in response to fluid injection (Cornet et al., 1997; Duboeuf et al., 2017; Guglielmi et al., 2015; Scotti & Cornet, 1994; Wei et al., 2015). While induced earthquakes have been located anywhere from a few meters to tens of kilometers from injection wells (Goebel & Brodsky, 2018), the spatial extent of fluid-induced aseismic slip is not as well characterized due to the paucity of direct observations. Understanding what conditions lead to seismic versus aseismic and localized versus widespread fault reactivation is central to physics-based hazard forecasting.

An outstanding opportunity to investigate these questions is offered by a decametric-scale fluid injection experiment recently conducted in an underground tunnel intercepting a dormant fault in a carbonate formation (Guglielmi et al., 2015) (Figure 1A). During the experiment, the fluid pressure and fault slip were recorded at the injection site. Although the observed slip was mostly aseismic, it is important to understand if the observations contained sufficient information to determine whether slip would have accelerated into an earthquake rupture if injection had

continued. Previous efforts to model the field experiment with a slip-weakening friction law concluded that aseismic slip outgrew the pressurized zone, potentially leading to a runaway earthquake with continued injection (Bhattacharya & Viesca, 2019).

Here, we use the data from the field experiment to examine the issue of slow and confined vs. fast and runaway slip in models with more realistic, laboratory-derived rate-and-state friction laws (Dieterich, 2007) consistent with laboratory results on materials from this specific fault zone (Cappa et al., 2019). Furthermore, we use the modeling to identify promising avenues to quantify the fault properties and control injection-induced seismicity hazard. We adopt a fully-dynamic computational framework that resolves both aseismic and seismic slip on faults. We keep other model ingredients relatively simple to better understand frictional effects in the presence of a diffusing fluid. For example, we do not explicitly model the change in fault permeability induced by slip as in previous studies (Bhattacharya & Viesca, 2019; Cappa et al., 2019; Guglielmi et al., 2015). Nonetheless, we find that multiple frictional scenarios of varying spatial behavior and proneness to large earthquakes match the slip observations of the field experiment equally well during fault pressurization. We also find that depressurization provides further constraints that could help identify potentially hazardous faults.

2 A unique fluid-injection experiment on a natural fault

The unprecedented field experiment involved injecting water directly into the fault zone and measuring the resulting fault slip at a depth of 280 m with a specially designed borehole probe (Guglielmi et al., 2015) (Figure 1B). Prior to the experiment, the shear and normal stress acting on the fault were estimated at 1.65 +/- 0.5 and 4.25 +/- 0.5 MPa, and the permeability and bulk modulus of the fault at 7×10^{-12} m^2 and 13.5 +/- 3.5 GPa, respectively. Figure 1C summarizes the main observations of the experiment, including the deceleration of slip

A. Field Experiment Setting

B. Field Experiment Setup

C. Field Experiment Results
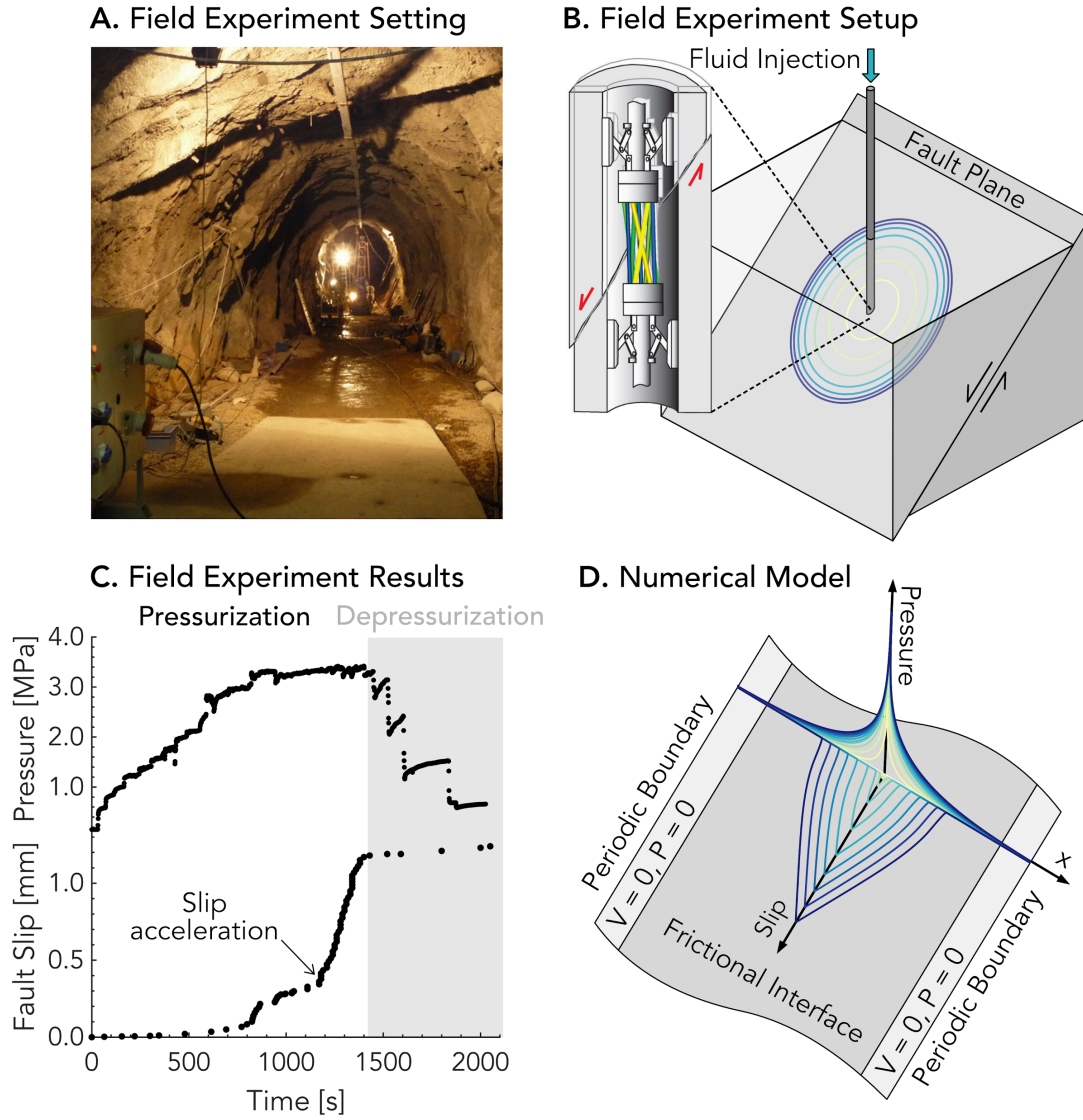
D. Numerical Model

Figure 1. In situ measurement and modeling of fault slip induced by fluid injection. (A) Setting of the field experiment in a tunnel intercepting a natural fault at 280 m (Photo courtesy of Yves Guglielmi). (**B**) Schematic of the field experiment presented in Guglielmi et al. (2015) in which fluid injected into a borehole crossing a natural but inactive fault caused its reactivation. A special borehole probe was used to measure the fault displacements directly at the injection site. (**C**) Pressure and fault slip measured during the field experiment. The grey area indicates the depressurization stage that has not been shown nor modeled in prior studies. (**D**) Schematic of the model used to simulate slip on a fault plane embedded in an elastic bulk medium. Snapshots of a sample fluid pressure diffusion scenario and its resulting fault slip are shown for illustration (the darker colors indicate later times). Schematics (**B**) and (**D**) are not to scale.

associated with depressurization not discussed in previous works. Remarkably, aseismic slip

undergoes a sharp acceleration without any significant increase in injection pressure at 1200 s.

Hydromechanical modeling suggests that 70% of the 20-fold increase in permeability during the

experiment occurred prior to this acceleration (Guglielmi et al., 2015). Laboratory experiments were also performed on grinded materials from the fault zone to further constrain the frictional properties (Cappa et al., 2019).

3 Numerical modeling of the field experiment

We model the field experiment as a fluid injection into a planar fault embedded in an elastic medium. As fluid pressure diffuses radially into the fault plane with hydraulic diffusivity α, fault friction eventually decreases and measurable slip ensues (Figure 1D). Slip is simulated with a fully-dynamic model of a rate-and-state fault that has been extensively used to study natural earthquakes and slow slip sequences (Lapusta et al., 2000; Noda & Lapusta, 2013) (supporting information). At steady state, the friction coefficient f depends on the slip rate V as $f = f^* + (a\text{-}b)\ln(V/V^*)$ where f^* is the value of f at reference slip rate V^* and $a\text{-}b$ quantifies the steady-state dependence of f on slip rate (Dieterich, 2007). By choosing V^* to be approximately the fastest slip rate measured during the field experiment ($V^* = 10^{-6}$ m/s), we make f^* into an estimate of the quasi-static residual steady-state friction f^r reached at the latest stages of the fault pressurization experiment. The difference between the residual and initial friction, $f^r - f_{ini}$, controls the elastic energy available to drive fault rupture once initiated (Galis et al., 2017; Garagash & Germanovich, 2012). Note that this is distinct from the difference between peak and initial friction, $f^p - f_{ini}$ (e.g., Gischig, 2015), which controls the timing of fault reactivation (supporting information).

3.1 Models in agreement with the observations during pressurization

The pressurization stage of the experiment (up to 1400 s) is equally well reproduced by a family of models. We investigate fault models with varying quasi-static residual friction f^*, as its value is not known from the field experiment and has been shown to affect the extent of the

slipping zone (Bhattacharya & Viesca, 2019; Dublanchet, 2019; Galis et al., 2017; Garagash & Germanovich, 2012). We find multiple scenarios with f^* between 0.48 and 0.60, $f_{ini} = 0.54$ and α between 0.04 and 0.85 m^2/s that match the slip observed during the pressurization period. Three representative cases are shown in Figures 2A-C and S6. Each f^*, a-b and α combination was selected to match the amplitude and slope of the slip acceleration at 1200 s (supporting information) and the lowest and highest α are consistent with the initial and final permeabilities, respectively, inferred by Guglielmi et al. (2015). As expected, the lower the residual friction and rate-weakening and the higher the hydraulic diffusivity, the sharper the acceleration (Figure S15-18). The remaining model parameters (Table S1) are determined from the timing of the initiation of significant slip at ~400 s and slip acceleration at ~1200 s, as described by the relationships derived in the supporting information. While the friction evolution in our model is governed by combined slip-rate and state-variable effects (Figure S6), the resulting evolution of friction coefficient vs. slip reveals that friction goes through a peak at the initiation of significant slip, followed by weakening with slip down to the steady-state constant value at the fastest slip rates of 10^{-6} m/s measured in the experiments (Figure 2B); the level of this residual friction with respect to initial fault prestress is an important factor controlling the extent of the fault slip zone with respect to the pressurized zone, as we discuss in the following.

Although the three models exhibit comparable slip histories at the injection site, they differ in features that were not directly accessible to field observation. In particular, their spatial behaviors differ qualitatively (Figure 3, S7-S10). Defining the pressurized zone with 0.5 MPa pressure contours as in previous works, the lower-friction scenario produces an aseismic front that outruns the pressurized region, within 1400 s, as in slip-weakening models (Bhattacharya & Viesca, 2019) (Figure 3D). By contrast, in the higher-friction model, which reproduces the
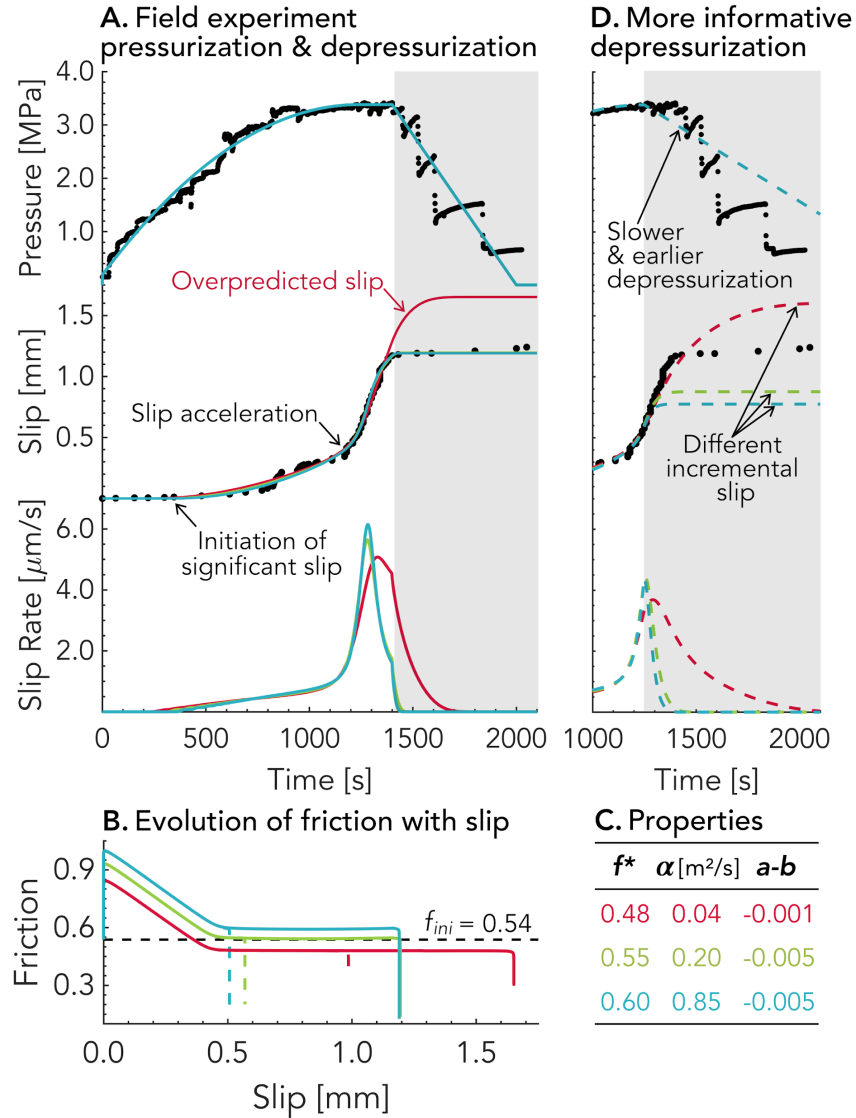
Figure 2. Multiple simulated scenarios match the pressurization stage of the experiment but respond differently to depressurization. (A) Temporal evolution of pore fluid pressure, slip and slip rate for three model scenarios (solid curves) that reproduce the observations (black dots) during the field-experiment pressurization up to 1400 s. **(B)** Simulated evolution of friction with slip at the injection site; the three scenarios correspond to lower (red), intermediate (green), and higher (blue) residual friction in comparison to the fault prestress (black dashed line). **(C)** Key frictional and hydraulic properties of the three scenarios. Note that only the intermediate and higher-friction faults result in slip consistent with the depressurization part. **(D)** Similar to (A) but for an improved depressurization: Reducing injection pressure once slip starts to accelerate would allow to distinguish between all three cases, helping to constrain the fault friction properties.

observations equally well, aseismic slip remains confined well within the pressurized area

(Figure 3F). In all of the models considered, the spatial extent of the slipping zone at the onset of

slip acceleration is well-estimated by a length scale h_{ac}, derived in the supporting information

(equation S13), which, remarkably, depends only on the quantities at the injection site (Figure 3D-F; Figure S11-S14). Our models clearly demonstrate that slip did not necessarily extend beyond the pressure perturbation during the experiment; that explaining a slip history at a single point in space is a non-unique problem; and that further hydro-mechanical complexity is not required to explain the observed slip to first order. Monitoring fault slip and fluid pressure along the length of the fault, directly with additional probes or remotely with geophysical methods, would help distinguish between these different scenarios and would allow to study additional fault processes such as permeability evolution and inelastic dilatancy (Segall & Rice, 1995).
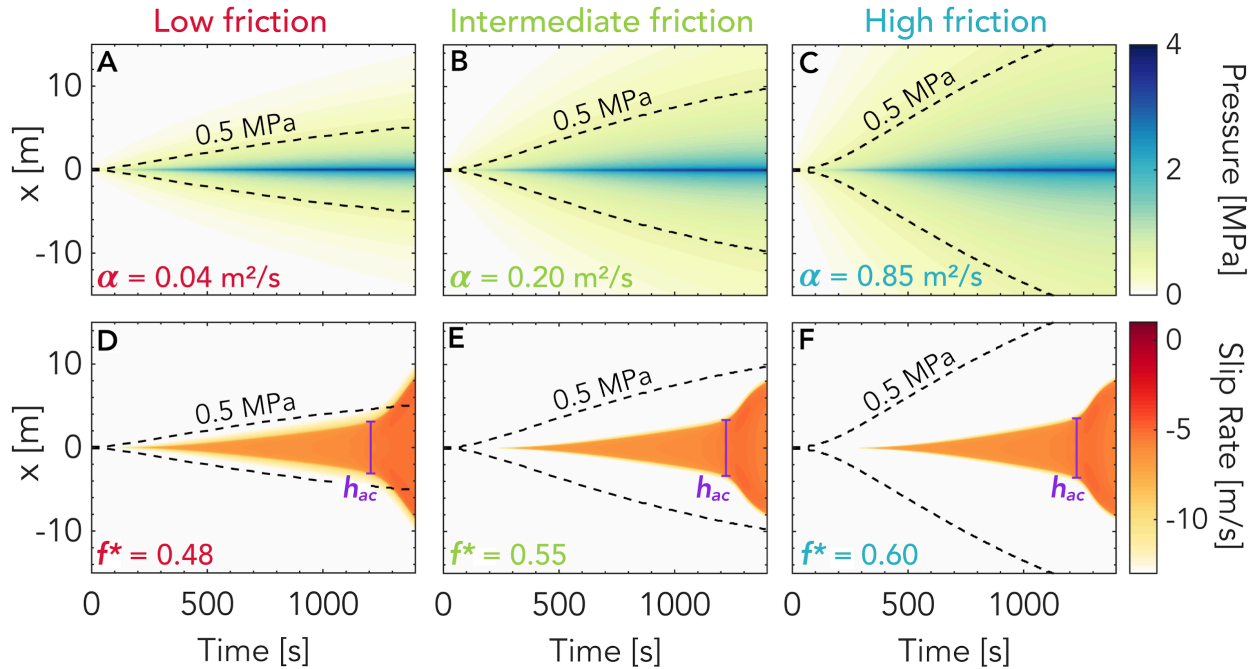

Figure 3. Whether the slipping zone is contained within or outruns the pressurized zone depends on fault friction. Spatial and temporal evolution of (**A-C**) pore fluid pressure and (**D-F**) slip rate for the three scenarios of Figure 2 during pressurization. The purple line shows the estimate h_{ac} of the slipping zone for the acceleration stage (see Supporting Information). Black dashed lines indicate the extent of the pressurized zone defined by 0.5 MPa fluid pressure contours. During the pressurization stage, the slipping zone of the lower-friction case outruns the pressurized zone while the intermediate- and higher-friction cases remain confined to the pressurized zone.

3.2 Distinguishing between models with depressurization

We find that the depressurization stage of the field experiment, which was not discussed or modeled in previous studies (Bhattacharya & Viesca, 2019; Cappa et al., 2019; Derode et al., 2015; Guglielmi et al., 2015), contains valuable information on fault properties. In this pressure-reduction stage, the lower-friction model features a pronounced delayed slip response that is not observed in the experiment or in the other two cases (Figure 2A). The intermediate- and higher-friction models, which also have higher hydraulic diffusivities, thus explain the entire set of observations better than the lower-friction model. Further discriminating between these two models is not possible with the current dataset because, by the time depressurization is initiated, the slip rates in these simulations are too low to produce a detectable difference in incremental slip (Figure 2A). However, if the injection pressure is decreased more gradually and earlier in the acceleration phase – at which point the intermediate- and higher-friction scenarios have approximately the same (and higher) slip rate – the three scenarios lead to diverging levels of incremental slip (Figure 2D). Our modeling thus demonstrates how timely depressurization could provide additional constraints on the frictional and hydromechanical properties of a fault zone.

The intermediate- and higher-friction cases are also consistent with prior information about the fault zone and laboratory studies. Indeed, laboratory experiments on the grinded fault zone material point to quasi-static residual friction values between 0.55 and 0.65 (Cappa et al., 2019). A hydraulic diffusivity between 0.20 and 0.85 m^2/s is consistent with the slip-enhanced permeability inferred by Guglielmi et al. (2015), suggesting that later enhanced permeabilities might be most relevant to explain the first order behavior of the fault. Finally, the initial fault conditions implied by these higher-friction cases are fully consistent with those of a dormant fault whereas the low-friction case is not (supporting information). Our preferred model for the

site of the injection experiment is thus a rate-weakening fault with $0.55 < f^* < 0.60$, $0.20 < \alpha <$

0.85 m^2/s, $a = 0.011$ and $b = 0.016$.

3.3 Diverging fault stability with sustained injection

Modeling what would have happened if the fluid injection had continued for longer

highlights why distinguishing between the three qualitatively different scenarios identified in this

study is crucial. In response to an extended constant-pressure injection (Figure 4, Figures S20-

S23), the low-friction fault nucleates an earthquake almost immediately, while the intermediate

and higher-friction faults decelerate and continue slipping aseismically before eventually

transitioning to seismic slip rates. Once a seismic rupture initiates, whether it is self-arrested or

run-away depends on the *dynamic* residual friction, f_d, which is generally slightly lower than f

(Galis et al., 2017; Garagash & Germanovich, 2012). If $f_d < f_{ini}$, as in the low- and intermediate-

friction cases (Figure 4B), the rupture may release enough elastic energy to propagate beyond the

fluid-affected regions and would only be stopped by less favorably stressed fault patches,

geometrical barriers, or more stable materials not present in the current model (Figures 4C,D).

Such runaway ruptures may be preceded by smaller ruptures or aseismic slip transients (Figures

S15 and S19); indeed, in fracture mechanics models (Galis et al., 2017), the transition to

runaway rupture requires a certain balance between fluid pressurization and background stress to

be reached. If $f_d > f_{ini}$, as in the high-friction case, the rupture self-arrests once out of the

pressurized zone (Figure 4E). For low- to intermediate-friction faults, the maximum expected

earthquake magnitude, M_{max}, is thus controlled by hydro-mechanical and geometrical fault

properties as opposed to injection attributes (e.g., cumulative volume injected) (van der Elst et

al., 2016; Galis et al., 2017; Gischig, 2015; McGarr, 2014). For example, varying the injection

rate in our simulations does not alter the event size (Figure S24). In the intermediate-friction
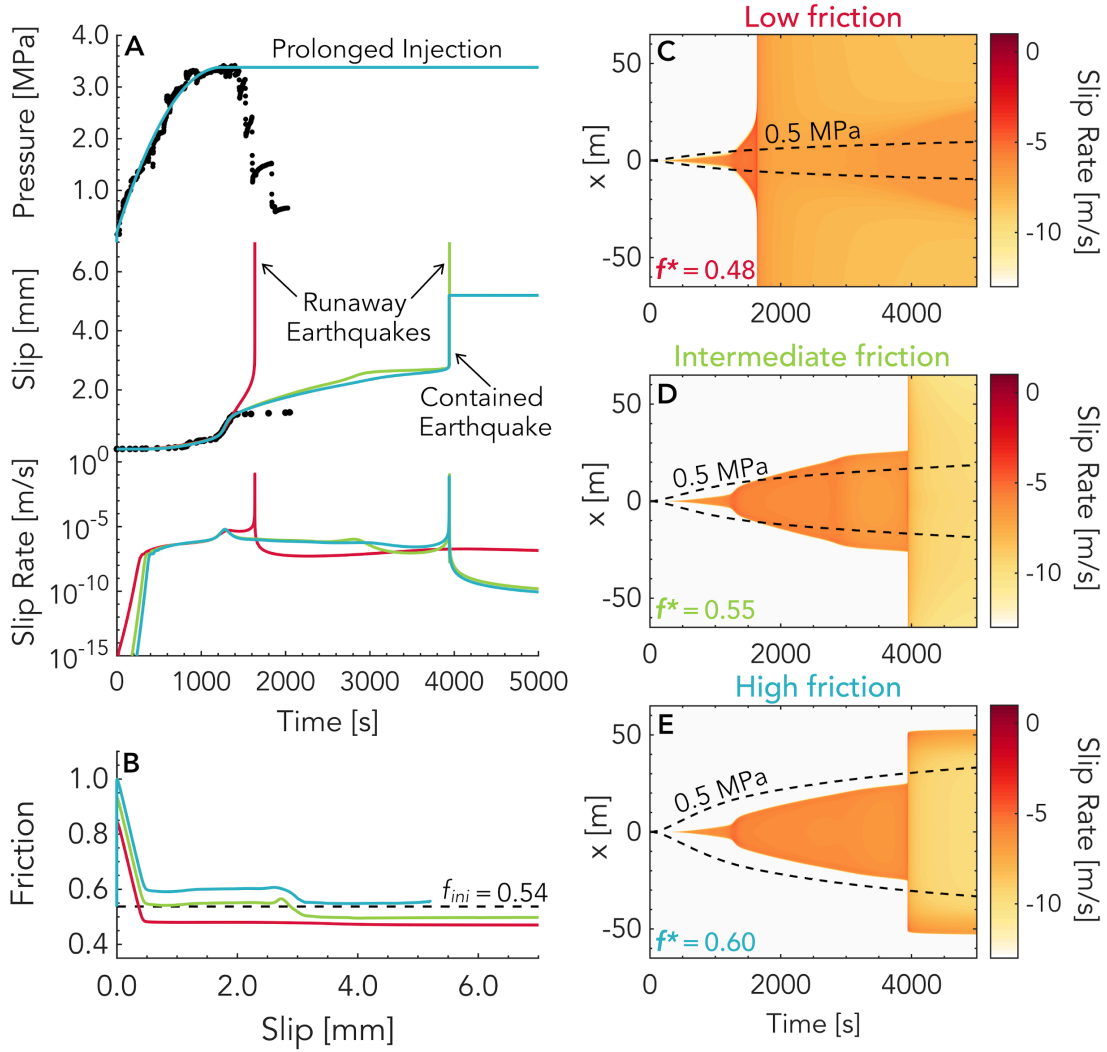
Figure 4. Prolonged injection reveals the diverging stability of the different fault models. Same as Figure 2 **(A-B)** and Figure 3 **(C-E)** but for a longer injection scenario, with keeping the pressure at the center of the fault constant past 1400 s instead of decreasing it. The low-friction case (red in A, C) produces a runaway earthquake rupture much sooner than the intermediate-friction case (green in A, D), while the higher-friction case (blue in A, E) - which is consistent with most known information about the fault - results in a self-arresting earthquake confined to the pressurized zone (blue).

case, the fault ultimately undergoes a runaway earthquake despite having stably released energy for over an hour, thus demonstrating that aseismic slip does not signify an absence of earthquake hazard. Fortunately, comparing the depressurization and prolonged injection scenarios reveals that reducing the injection pressure might be sufficient to suppress earthquake nucleation at the injection site. The lower-friction the fault, the faster the rate of this depressurization needs to be

(Figure S25). Note, however, that earthquakes could still be triggered by aseismic slip itself on more unstable heterogeneities away from the injection site (Eyre et al., 2019; Guglielmi et al., 2015).

4 Discussion and Conclusions

To summarize, our modeling of a fluid-injection experiment into a fault zone reveals that the difference between fault prestress and quasi-static or dynamic fault friction controls whether slip is confined to the fluid-affected zone or outruns it. We find that: (i) multiple scenarios of different friction levels are consistent with the measured slip at the injection site during the pressurization phase, (ii) the low-friction scenario in which slow slip outruns the pressurized region is inconsistent with slip during the depressurization phase, and (iii) the high-friction scenario, in which the slipping zone is well confined within the pressurized region, is most consistent with the full range of information from the experiment, including the fault behavior during fault depressurization and laboratory friction measurements on the materials from the fault zone. Key hydro-mechanical parameters such as the ratio of quasi-static friction to initial normalized prestress, f^*/f_{ini}, the rate dependence of friction, a-b, and the hydraulic diffusivity, α, exercise a first-order control on the stability and spatial extent of a fault response to fluid injections. Further constraining these parameters is thus critical for seismic hazard management. In the geoenergy industry, test injections with timely depressurization and spatiotemporal monitoring of fluid pressure and aseismic slip could be performed prior to exploitation to ensure that there are no low-friction faults nearby. Our findings show that augmenting fault-pressurization experiments with suitably designed depressurization phases and multiple monitoring locations along the fault would provide invaluable insight into the physics of both induced and natural earthquakes (Savage et al., 2017) and friction properties of dormant faults.

Such more advanced injection experiments and corresponding modeling work will potentially be able to assess the effects and relative importance of additional mechanisms (e.g., poroelastic stresses (Deng et al., 2016; Goebel et al., 2017; Segall & Lu, 2015), slip-induced dilatancy (Cappa et al., 2019; Segall & Rice, 1995), bulk fluid diffusion, and enhanced dynamic weakening) and complexity (e.g., material heterogeneities (Eyre et al., 2019)).

Acknowledgments

References

Bhattacharya, P., & Viesca, R. C. (2019). Fluid-induced aseismic fault slip outpaces pore-fluid migration. *Science (New York, N.Y.)*, *364*(6439), 464–468. https://doi.org/10.1126/science.aaw7354

Cappa, F., Scuderi, M. M., Collettini, C., Guglielmi, Y., & Avouac, J.-P. (2019). Stabilization of fault slip by fluid injection in the laboratory and in situ. *Science Advances*, *5*(3), eaau4065. https://doi.org/10.1126/sciadv.aau4065

Cornet, F. H., Helm, J., Poitrenaud, H., & Etchecopar, A. (1997). Seismic and Aseismic Slips Induced by Large-scale Fluid Injections. In *Seismicity Associated with Mines, Reservoirs and Fluid Injections* (pp. 563–583). Basel: Birkhäuser Basel. https://doi.org/10.1007/978-3-0348-8814-1_12

Deng, K., Liu, Y., & Harrington, R. M. (2016). Poroelastic stress triggering of the December 2013 Crooked Lake, Alberta, induced seismicity sequence. *Geophysical Research Letters*, *43*(16), 8482–8491. https://doi.org/10.1002/2016GL070421

Derode, B., Guglielmi, Y., De Barros, L., & Cappa, F. (2015). Seismic responses to fluid pressure perturbations in a slipping fault. *Geophysical Research Letters*, *42*(9), 3197–3203. https://doi.org/10.1002/2015GL063671

Dieterich, J. H. (2007). Applications of Rate- and State-Dependent Friction to Models of Fault Slip and Earthquake Occurrence. *Treatise on Geophysics*, 107–129. https://doi.org/10.1016/B978-044452748-6.00065-1

Dublanchet, P. (2019). Fluid driven shear cracks on a strengthening rate-and-state frictional fault. *Journal of the Mechanics and Physics of Solids*, *132*, 103672. https://doi.org/10.1016/j.jmps.2019.07.015

Duboeuf, L., De Barros, L., Cappa, F., Guglielmi, Y., Deschamps, A., & Seguy, S. (2017). Aseismic Motions Drive a Sparse Seismicity During Fluid Injections Into a Fractured Zone in a Carbonate Reservoir. *Journal of Geophysical Research: Solid Earth*, *122*(10), 8285–8304. https://doi.org/10.1002/2017JB014535

Ellsworth, W. L. (2013). Injection-Induced Earthquakes. *Science*, *341*(6142), 1225942. https://doi.org/10.1126/science.1225942

van der Elst, N. J., Page, M. T., Weiser, D. A., Goebel, T. H. W., & Hosseini, S. M. (2016). Induced earthquake magnitudes are as large as (statistically) expected. *Journal of Geophysical Research: Solid Earth*, *121*(6), 4575–4590. https://doi.org/10.1002/2016JB012818

Eyre, T. S., Eaton, D. W., Garagash, D. I., Zecevic, M., Venieri, M., Weir, R., & Lawton, D. C. (2019). The role of aseismic slip in hydraulic fracturing–induced seismicity. *Science Advances*, *5*(8), eaav7172. https://doi.org/10.1126/sciadv.aav7172

Galis, M., Ampuero, J. P., Mai, P. M., & Cappa, F. (2017). Induced seismicity provides insight into why earthquake ruptures stop. *Science Advances*, *3*(12), eaap7528. https://doi.org/10.1126/sciadv.aap7528

Garagash, D. I., & Germanovich, L. N. (2012). Nucleation and arrest of dynamic slip on a pressurized fault. *Journal of Geophysical Research: Solid Earth*, *117*(B10). https://doi.org/10.1029/2012JB009209

Gischig, V. S. (2015). Rupture propagation behavior and the largest possible earthquake induced by fluid injection into deep reservoirs. *Geophysical Research Letters*, *42*(18), 7420–7428. https://doi.org/10.1002/2015GL065072

Goebel, T.H.W., Weingarten, M., Chen, X., Haffener, J., & Brodsky, E. E. (2017). The 2016 Mw5.1 Fairview, Oklahoma earthquakes: Evidence for long-range poroelastic triggering at >40 km from fluid disposal wells. *Earth and Planetary Science Letters*, *472*, 50–61.

https://doi.org/10.1016/J.EPSL.2017.05.011

Goebel, Thomas H W, & Brodsky, E. E. (2018). The spatial footprint of injection wells in a global compilation of induced earthquake sequences. *Science (New York, N.Y.)*, *361*(6405), 899–904. https://doi.org/10.1126/science.aat5449

Grigoli, F., Cesca, S., Priolo, E., Rinaldi, A. P., Clinton, J. F., Stabile, T. A., et al. (2017). Current challenges in monitoring, discrimination, and management of induced seismicity related to underground industrial activities: A European perspective. *Reviews of Geophysics*, *55*(2), 310–340. https://doi.org/10.1002/2016RG000542

Guglielmi, Y., Cappa, F., Avouac, J. P., Henry, P., & Elsworth, D. (2015). Seismicity triggered by fluid injection-induced aseismic slip. *Science*, *348*(6240). https://doi.org/10.1126/science.aab0476

Lapusta, N., Rice, J. R., Ben-Zion, Y., & Zheng, G. (2000). Elastodynamic Analysis for Slow Tectonic Loading with Spontaneous Rupture Episodes on Faults with Rate-and State-dependent Friction. *Journal of Geophysical Research*, *105*(B10), 765–788. https://doi.org/10.1029/2000JB900250

McGarr, A. (2014). Maximum magnitude earthquakes induced by fluid injection. *Journal of Geophysical Research: Solid Earth*, *119*(2), 1008–1019. https://doi.org/10.1002/2013JB010597

McGarr, A., Bekins, B., Burkardt, N., Dewey, J., Earle, P., Ellsworth, W., et al. (2015). Coping with earthquakes induced by fluid injection. *Science*, *347*(6224), 830 LP – 831. https://doi.org/10.1126/science.aaa0494

Noda, H., & Lapusta, N. (2013). Stable creeping fault segments can become destructive as a result of dynamic weakening. *Nature*, *493*(7433), 518–521. https://doi.org/10.1038/nature11703

Savage, H. M., Kirkpatrick, J. D., Mori, J. J., Brodsky, E. E., Ellsworth, W. L., Carpenter, B. M., et al. (2017). Scientific Exploration of Induced SeisMicity and Stress (SEISMS). *Scientific Drilling*, *23*, 57–63. https://doi.org/10.5194/sd-23-57-2017

Scotti, O., & Cornet, F. H. (1994). In Situ Evidence for fluid-induced aseismic slip events along fault zones. *International Journal of Rock Mechanics and Mining Sciences & Geomechanics Abstracts*, *31*(4), 347–358. https://doi.org/10.1016/0148-9062(94)90902-4

Segall, P., & Lu, S. (2015). Injection-induced seismicity: Poroelastic and earthquake nucleation effects. *Journal of Geophysical Research: Solid Earth*, *120*(7), 5082–5103. https://doi.org/10.1002/2015JB012060

Segall, Paul, & Rice, J. R. (1995). Dilatancy, compaction, and slip instability of a fluid-infiltrated fault. *Journal of Geophysical Research: Solid Earth*, *100*(B11), 22155–22171. https://doi.org/10.1029/95JB02403

Wei, S., Avouac, J.-P., Hudnut, K. W., Donnellan, A., Parker, J. W., Graves, R. W., et al. (2015). The 2012 Brawley swarm triggered by injection-induced aseismic slip. *Earth and Planetary Science Letters*, *422*, 115–125. https://doi.org/10.1016/j.epsl.2015.03.054

Supporting Information References

Dieterich, J. H. (1992). Earthquake nucleation on faults with rate-and state-dependent strength. Tectonophysics, 211(1–4), 115–134. https://doi.org/10.1016/0040-1951(92)90055-B

Helmstetter, A., & Shaw, B. E. (2009). Afterslip and aftershocks in the rate-and-state friction law. Journal of Geophysical Research: Solid Earth, 114(B1). https://doi.org/10.1029/2007JB005077

Rubin, A. M., & Ampuero, J.-P. (2005). Earthquake nucleation on (aging) rate and state faults. Journal of Geophysical Research: Solid Earth, 110(B11). https://doi.org/10.1029/2005JB003686

Uenishi, K., & Rice, J. R. (2003). Universal nucleation length for slip-weakening rupture instability under nonuniform fault loading. Journal of Geophysical Research: Solid Earth, 108(B1). https://doi.org/10.1029/2001JB001681

Viesca, R. C., & Rice, J. R. (2012). Nucleation of slip-weakening rupture instability in landslides by localized increase of pore pressure. Journal of Geophysical Research: Solid Earth, 117(B3). https://doi.org/10.1029/2011JB008866